Check for updates

Functionalised graphite felt anodes for enhanced power generation in membrane-less soil microbial fuel cells†

Simran Kaur Dhillon, [ID] [ab] Jakub Dziegielowski,[a] Patit Paban Kundu [ID] *[b] and Mirella Di Lorenzo [ID] *[a]

There is a global need for sustainable and clean technologies that can actively contribute to reach the net-zero carbon goal by 2050. In this context, Soil Microbial Fuel Cell (SMFC) technology has a huge potential as an affordable and green energy harvesting source and as a carbon-neutral bioremediation strategy for the treatment of polluted lands. In this work, for the first time, cobalt oxide (Co_3O_4) modified graphite felt (GF) electrodes are explored as the anode material in SMFCs, with the aim of promoting the development of a high-performing electroactive biofilm and, therefore, boosting electrogenesis. First, cobalt hydoxide salt are hydrothermally distributed onto the graphite felt electrodes, then Co_3O_4 nanoflowers are obtained by calcination. The resulting Co_3O_4–GF electrodes show lower hydrophobicity and higher conductivity than GF, however, when Co_3O_4–GF is tested as the anode of a membrane-less, air-cathode SMFC device, after an initial boost in power performance, the activity decays with time, probably due to Co_3O_4 leaching. To overcome this issue, Co_3O_4 –GF electrodes are interweaved with polyaniline (PANI), resulting in PANI–Co_3O_4–GF, for a much more stable SMFC system, which generates a peak power density of 70 mW m^{-2} at a current density of 143 mA m^{-2}. This value of power density is nearly three times greater than the power generated by the same SMFC system with a plain GF anode. The interweaving of PANI onto the Co_3O_4–GF electrode leads to a porous structure that, while providing stability to the electrode over prolonged periods of operation, also favours microbial attachment. Overall, these results provide exciting perspectives on the development of composite carbon-based anode materials for high performing soil microbial fuel cells, thus inspiring future trends in the field.

Sustainability spotlight

We are facing unprecedent times of crisis on multiple fronts. Energy demands are rising to respond to the needs of an ever-expanding population that poses serious threats to the resilience of cities. Land pollution is one of the sad outcomes of this situation. Soil microbial fuel cell technology provides a very attractive opportunity for clean and emission-free energy production and sustainable bioremediation of contaminated soil. In this study, we investigate the use of carbon-based composite electrode materials to enhance the electrochemical performance of this technology and help its progress towards practical implementations. Our work is primarily aligned with the UN SDGs 7, 11, but it is also related to the UN SDGs 15 and 13.

1. Introduction

To contrast the devastating effects of climate change, we must increase our reliance on low-carbon emission technologies and move away from fossil fuels. According to the World Economic Forum, decarbonization, which refers to the reduction of carbon dioxide emissions resulting from human activity in the atmosphere, is the only solution to climate stabilization. Microbial fuel cell technology can help address this global emergency by providing a net-zero carbon, sustainable and cost-effective solution.[1] Microbial fuel cell technology generates electricity through microbial degradation of organic substrates from low-value energy sources, including wastewaters, to H_2O and CO_2.[2] Amongst the several types of microbial fuel cell designs, soil microbial fuel cells (SMFCs) are particularly attractive, given the simplicity of design, the long-term stability and the minimum maintenance required, which facilitates remote applications.[3] SMFCs also offer attractive perspectives for self-powered soil bioremediation;[4] organic pollutants in soils are degraded at the anode *via* the action of endogenous microorganisms, and the electrons generated throughout the

[a]Department of Chemical Engineering, Centre for Biosensors, Bioelectronics & Biodevices (C3Bio), University of Bath, Claverton Down, BA2 7AY, UK. E-mail: m.di.lorenzo@bath.ac.uk

[b]Department of Chemical Engineering, Indian Institute of Technology, Roorkee, 247667, India. E-mail: patit.kundu@ch.iitr.ac.in

process are transported to the cathode *via* an external circuit, thus producing electricity. At the cathode, the electrons participate in the oxygen reduction reaction (ORR) together with the protons generated at the anode, which are transferred to the cathode across the soil matrix.[5] As the redox reactions proceed, a potential gradient develops, favouring power generation and bioremediation processes.[6] Soil characteristics, such as availability of liable organics, endogenous microbial communities, water content, and pH, markedly influence the electrochemical performance of the SMFC.[5] Design factors, such as electrode configuration and orientation, also influence the electroactive efficiency of SMFCs.[7]

The anode material influences the development of the electroactive biofilm and, therefore, the overall performance of the SMFC.[8] Carbonaceous materials, including carbon paper, carbon felt, and graphite felt, have been extensively exploited in microbial fuel cells.[9–11] In microbial fuel cells, carbon electrodes are preferred over metal-based ones as they are cost-effective and also facilitate the attachment and growth of biofilms, due to their high biocompatibility, specific surface area and roughness.[12–14] In SMFCs, carbon-based additives such as biochar[15] and carbon fibers[16] can be added to the soil to overcome charge transfer limitations. Graphite felt (GF) is a particularly popular electrode material in microbial fuel cells due to its 3D structure with a high specific surface area.[17] A recent study compared the performance of SMFCs with graphite felt as the cathode against different anodes such as graphite felt, aluminium sheet, activated carbon felt, graphite paper, and carbon cloth. After 115 days of continuous operation, SMFCs with graphite felt as the cathode and anode electrode, generated the greatest cell potential and power density compared to other 2D electrodes.[18] Nonetheless, GF has greater hydrophobicity compared to other carbon-based electrodes, which can limit microbial attachment and the effective development of electroactive biofilms.[19] Consequently, GF electrodes are typically acid treated to allow protonation of the –OH group onto the electrode surface and enhance electrostatic interactions.[20] The conductivity of carbon-based anodes can be enhanced with the use of metals.[21] For example, the functionalization of graphite felt with Fe_3O_4 and bentonite–Fe, led the power density generated by the SMFC to be, respectively, two times and three times higher than that in the case of pure graphite felt anodes.[22] Composite materials, consisting of carbon and transition metals such as Fe, Co, Ni, Fe, and Cu, offer an attractive anode material alternative for microbial fuel cells since they combine the benefits of carbon-based materials with the great conductivity of metal oxides for high electron transfer rates.[23–25] Among several options, cobalt oxide is particularly promising as an anode material, as it has been shown to reduce the hydrophobicity of GF and improve the interfacial charge transfer rates.[26,27] These benefits result from an enhanced specific surface area of the electrode thanks to the 3D structure of the Co_3O_4 nanoflowers combined with the generation of positively charged metal catalytic sites that promote the adhesion of negatively charged bacteria onto the electrode surface.[28]

In the development of carbon–metal composite electrode materials, porous conducting polymers can provide a matrix for the entrapment of the metal catalyst to prevent leaching and enhances stability while increasing electronic and ionic conductivity.[29] In particular, polyaniline (PANI) modified composites have been widely used in microbial fuel cells.[30–32] The interweaving of PANI with metals or metal oxides leads to conducting nanocomposites that, compared to conventional carbon electrodes, have a larger surface area, better catalytic activity, and, thus, can lead to better performing microbial fuel cells.[33] PANI can enhance the roughness of the electrode,[35] which has been reported as crucial for anode performance in microbial fuel cells.[36,37] Moreover, the positively charged PANI would attract negatively charged microorganisms at the anode facilitating their attachment;[38] PANI has been shown to allow direct electron transfer to the anode *via* redox centers in the outer membrane and mediators excreted by electroactive species like *Shewanella oneidensis*.[39,40]

In this study, we explore the use of graphite felt functionalized with cobalt oxide nanoflowers as the anode material in SMFCs. The cobalt oxide nanoflowers are obtained by calcinating cobalt hydroxide salt hydrothermally deposited onto graphite felt. The performance of the resulting Co_3O_4–GF electrode as the anode of an air-cathode and membrane-less SMFC is investigated and compared with a second type of composite anode material in which the Co_3O_4 nanoflowers on GF are embedded within a polyaniline structure (PANI–Co_3O_4–GF), to overcome the risk of poor electron transfer efficiency.[34] To the best of our knowledge, this is the first example of using a composite anode material, consisting of a conductive polymer and a transition metal oxide, in a soil microbial fuel cell system. The two composite anode electrodes, along with two controls, GF coated with PANI (PANI–GF) and GF, are physically and electrochemically characterized. This work paves the way for future development on composite anode materials based on cost-effective metal derivatives for high performing SMFC systems.

2. Materials and methods

2.1. Materials

All the reagents used were purchased from Sigma-Aldrich and were of analytical grade and used without further purification. $Co(NO_3)\cdot 6H_2O$ was purchased from Sigma-Aldrich. Aniline ≥99.5% and ammonium peroxodisulphate (APS) ≥98% were purchased from VWR chemicals. Graphite felt was purchased from Online Furnace Services Ltd, Scotland, UK. All aqueous solutions were prepared in deionised water.

The soil used in the study was collected from the University of Bath campus. No additives were used to improve the soil quality or organic content. After collection, the soil was manually sieved and cleaned of small stones, roots, and leaves. Table 1 summarises the properties of the soil used. An HI-3869 soil test kit by Hanna Instruments was used to test the elemental content, particularly nitrogen (N), phosphorous (P), and potassium, for soil quality analysis (soil test interpretation guide). The conductivity and pH of the soil were determined using a Thermo Scientific Orion Star A325 probe before the operation. To determine the moisture content of the soil, a measured

Table 1 Physicochemical parameters of the soil used in this study

Parameters	Measured values from laboratory tests
pH	6.8
Conductivity	1084 μS cm^{-1}
Nitrogen content	High
Phosphorous content	Low
Potassium content	Medium
Moisture content	28.75%
Organic matter content	5.52

amount of soil was oven dried at 105 °C for 24 h and the difference in the initial weight of the soil and the weight after thermal treatment was used according to eqn (1).

$$\% \text{ Moisture content} = \left(\frac{\text{initial weight} - \text{final weight}}{\text{final weight}} \right) \times 100$$

$$(1)$$

After moisture content analysis, the dried sample was further heated in a muffle furnace at 350 °C for another 24 h to obtain the organic matter content according to eqn (2).[3]

$$\% \text{ Organic content} = \left(\frac{W_{105} - W_{350}}{W_{105}} \right) \times 100 \qquad (2)$$

where W_{105} (g) is the weight of soil obtained after drying at 105 °C and W_{350} is the final weight (g) after drying at 350 °C.

2.2. Preparation of functionalized graphite felt anodes

Before modification, graphite felt (7 cm × 7 cm) was thoroughly washed by sequentially soaking it in 1 M HCl, 3% H_2O_2 and distilled water at 60 °C for 30 min each, and finally heated at 450 °C. Flower-like Co_3O_4 nanostructures were synthesized onto GF *via* a two-stage hydrothermal-calcination process, following previous work.[41] The resulting GF pieces were soaked in an aqueous solution containing 0.44 g of $Co(NO_3) \cdot 6H_2O$ and 0.42 g of urea and sonicated for 30 minutes to ensure a uniform concoction. The electrode suspension was transferred to a Teflon-lined hydrothermal reactor (150 mL) and maintained at 120 °C for 6 h in a hot-air oven. After cooling to room temperature, the GF pieces coated with cobalt hydroxide were carefully rinsed in distilled water and dried at 60 °C. Finally, calcination was performed at 300 °C in a muffle furnace for 3 h to obtain GF coated with Co_3O_4 nanoflowers (Co_3O_4–GF) (Fig. 1a). Fig. 1b and c provide, respectively, an overview of the electrodes tested in this study and the experimental set-up. The PANI–Co_3O_4–GF electrode was prepared by electro-polymerization of aniline onto the surface of Co_3O_4–GF electrodes in a three-electrode cell with a stainless steel mesh (7 cm × 7 cm) as a counter for an unhindered flow of electrons and Ag/AgCl as the reference electrode, respectively, using PalmSens4 potentiostat equipped with the PSTrace software. First, the surface of the Co_3O_4–GF electrode was activated by cyclic voltammetry (CV) at 50 mV s^{-1} for 5 cycles in a 0.7 M HNO_3 aqueous solution. Then, 0.4 M aniline was added to the acidic solution, followed by N_2 purging for 30 minutes before electropolymerization. The synthesis was initiated by
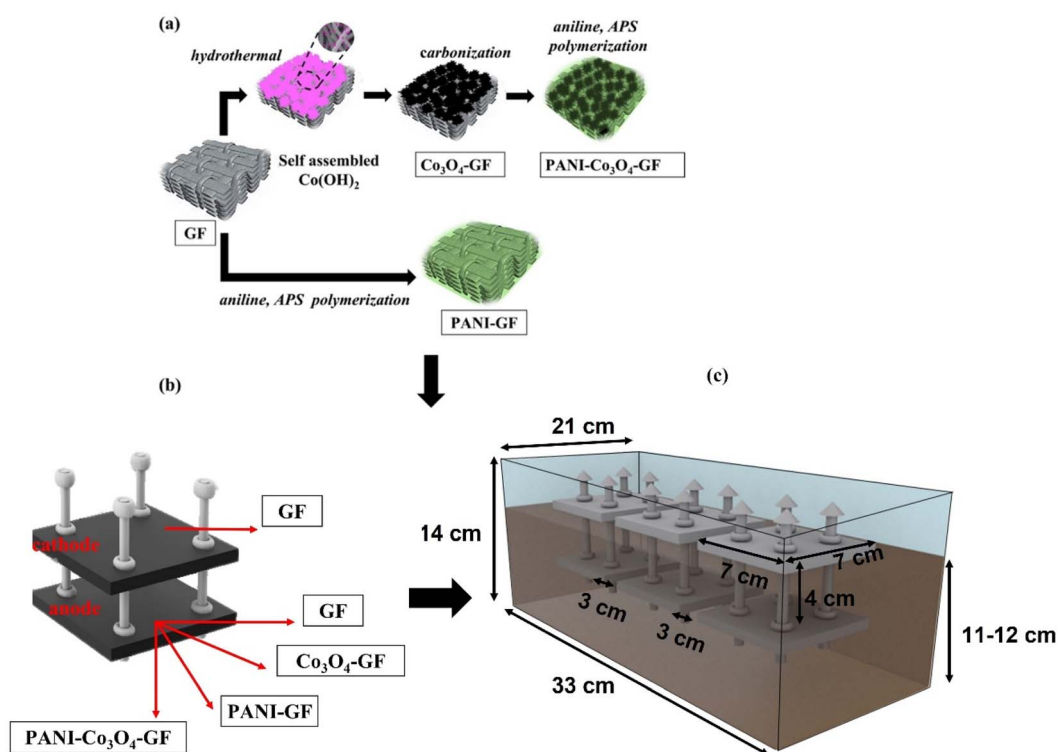

Fig. 1 Synthesis steps for the electrodes developed (a); SMFC design and overview of the electrodes tested in this study (b); and experimental set-up (c).

chronoamperometry at 0.75 V for 30 minutes.[42] The resulting electrode was rinsed with dilute HCl and distilled water, to remove any impurities, and dried overnight.

PANI–GF electrodes were also tested as a control. In this case, PANI was electro-polymerized (following the method described above) onto a GF electrode not functionalized with Co_3O_4.

2.3. Material characterization and electrochemical analysis

The structure of the generated electrodes was analyzed by X-ray diffraction (XRD, STOE STADI P), while Fourier transform-infrared spectroscopy (PerkinElmer FT-IR spectrometer) was performed to identify the surface functionalities of the electrodes within the wavelength range of 400–4000 cm^{-1}. Scanning electron microscopy (SEM, Hitachi SU3900) and elemental mapping were used to assess electrode material morphology and elemental distribution. The electrodes were gold-coated before the analysis. ImageJ software was used to analyse the SEM images generated. Contact angle measurements (Data-Physics OCA 25) were performed to assess the hydrophobicity of the electrodes. To examine the morphology of the anodic biofilm, after 4 months of operation the anodes were conditioned with 4% glutaraldehyde solution for 4 h, followed by dehydration in different concentrations of ethanol solution (25%, 50%, 75%, and 100%) at room temperature, each for 15 min.[43] The air-dried anodes were coated with gold by sputtering and analysed by SEM.

The electrochemical performance of the electrodes developed as the anode in an SMFC was investigated at different stages of batch operation by using Ag/AgCl as the reference electrode and the SMFC cathode (plain GF) as the counter electrode. The working electrode was cycled at 0.01 V s^{-1} within the potential window −0.5 V to 1 V for at least 15 min before data collection. Cyclic voltammetry (CV) and linear sweep voltammetry (LSV) measurements were recorded. Furthermore, the stability of the electrodes developed was determined by chronoamperometry (CA) at 0.25 V for 30 minutes after 30 days of operation to examine the effect of biofilm adhesion onto the electrode surface. Electrochemical impedance spectroscopy (EIS) was carried out in the frequency range 105 Hz to 0.1 Hz to assess the ohmic and charge transfer resistances of the several electrodes produced prior to being used as the anode in the SMFC. Tests were performed in a three-electrode set-up in 50 mM PBS, using the anode as the working electrode, Pt wire as the counter electrode and a Ag/AgCl electrode as the reference electrode. EIS measurements were also repeated after four months of operation to assess the effect that the anodic biofilm has on the electrode resistance. In this case, the tests were performed directly in the soil media where the SMFCs were operated, with the anode as the working electrode, the GF cathode as the counter electrode, and the Ag/AgCl electrode as the reference electrode.

2.4. Soil microbial fuel cell configuration and operation

Air-cathode, membrane-less SMFCs, which differed according to the anode material used, were constructed as previously described.[3] Briefly, the system consisted of an anode (7 × 7 cm), either GF, Co_3O_4–GF, PANI–Co_3O_4–GF, or PANI–GF, buried inside the soil, and a cathode (7 × 7 cm), made of untreated GF, placed onto the soil surface at a fixed distance from the anode of 4 cm, and it was exposed to air. Rectangular PVA containers (33 cm × 21 cm × 14 cm), filled with approximately 7–8 kg soil, were used to host three replicates of a specific SMFC type for a total of four PVA containers and 12 SMFCs tested. The moisture content in soil is a key factor for SMFC operation.[3] Accordingly, approximately 250 mL of tap water was sprinkled over the topsoil layer on a two-day basis to compensate for moisture loss due to evaporation. This helps maintain water saturation conditions in the soil while ensuring that the cathodes are not submerged in water. Titanium wire (0.25 mm, Alfa Aesar) intertwined within the electrodes was used to connect the anode and cathode to an external resistance of 510 Ω. Voltage drops (V) across each SMFC were recorded and collected using a data acquisition system (DAQ6510, Keithley instruments, Tektronix UK Ltd). Polarization tests were conducted by first operating the SMFCs at open circuit voltage for 12 h and then applying decreasing external loads (R), from 10 000 Ω, 5000 Ω, 1000 Ω, 700 Ω, 500 Ω, 300 Ω, and 100 Ω, at 10 min intervals using a resistor box (Cropico resistance decade box, resistance range 10 MΩ–10 Ω) and recording the output voltage and current. Current density (mA cm^{-2}) was calculated according to Ohm's law; $I = V/(RA)$, where V is the cell voltage (V) and A is the geometric anode area (49 cm^2). Power density (mW cm^{-2}) was calculated as $P = (IV)/A$.

3. Results and discussion

3.1. Physicochemical characterization studies of the anodes developed

In this study, four different types of graphite felt electrodes were tested as the anode in an air-cathode and membrane-less soil microbial fuel cell: plain graphite felt (GF), graphite felt coated with polyaniline (PANI–GF), graphite felt functionalized with cobalt oxide nanoflowers (Co_3O_4–GF), and graphite felt functionalized with cobalt oxide nanoflowers and coated with polyaniline (PANI–Co_3O_4–GF). The hydrophobicity of the four electrodes was investigated and compared. As expected, the functionalization of graphite felt with Co_3O_4 led to a decrease in the hydrophobicity, corresponding to a reduction of the contact angle to 116 ± 0.6° from a value of 139 ± 0.1° for plain GF (Fig. 2a). This improvement in the electrode wettability could be a consequence of the oxygen atoms introduced by Co_3O_4 that could alter the electrostatic field at the surface of graphite felt and facilitate interaction between the electrode material and water molecules.[28,44] The electrodeposition of PANI further decreased the surface hydrophobicity, with PANI–Co_3O_4–GF reaching a contact angle of 97 ± 0.9. The decrease in the electrode hydrophobicity resulting from the synergistic effect of Co_3O_4 and PANI, along with the porosity and high specific surface area achieved, promotes good contact between the electroactive biofilm and anode, thus enhancing electron transfer.[45,46]
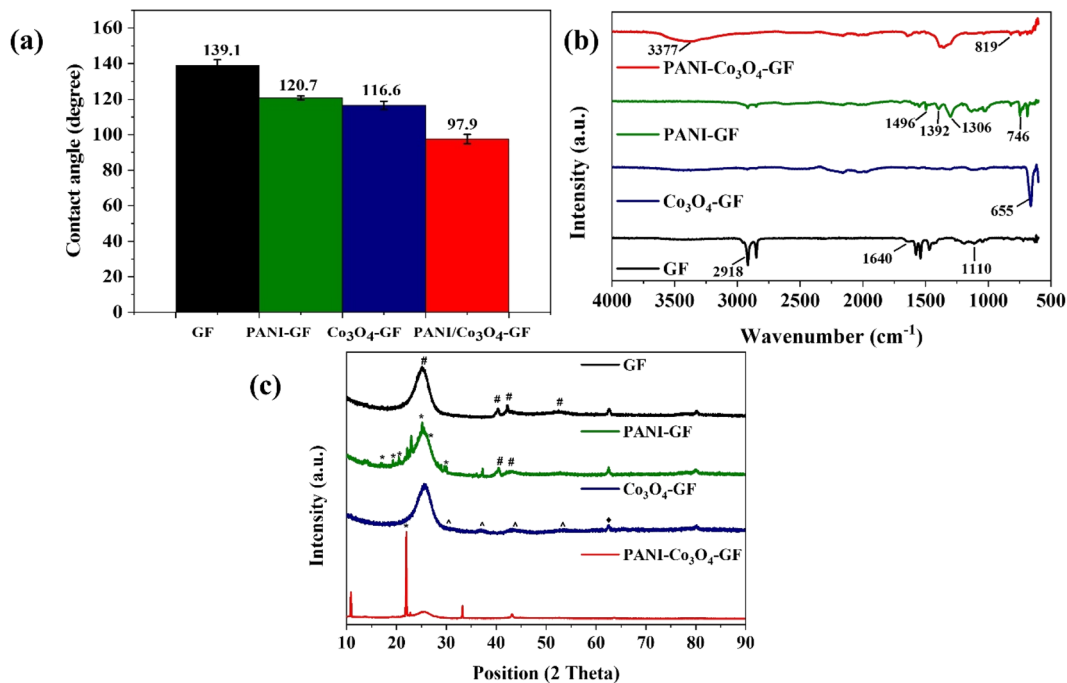
Fig. 2 Physicochemical analyses of the four anodes tested in this study. (a) Contact angle measurements, error bars account for the deviation in the measured angle at three different points on the electrode surface. (b) FTIR spectra. (c) XRD analysis.

FTIR spectroscopy analysis of the four electrodes was also carried out. Fig. 2b shows the spectra obtained for each anode material. All electrodes exhibit similar peaks over the wavenumber range 500–4000 cm^{-1}, which are associated with GF. However, the intensity of the peaks varied significantly with the surface modifications introduced. For all electrodes, absorption bands observed at around 1020 cm^{-1} (–CO), 1110 cm^{-1} (–COOH), 1640 cm^{-1} (–C=O), 2855 cm^{-1} (–CH), 2918 cm^{-1} (–CH), and 3377 cm^{-1} (–OH), belong to stretching vibrations of hydroxyl and carboxyl groups.[47] The peaks observed at 1579 cm^{-1} and 1476 cm^{-1} in the case of PANI–GF and PANI–Co$_3$O$_4$–GF are associated with C=C stretching vibrations of benzene and quinine rings due to polyaniline oxidation. Distinct peaks in the range of 650–500 cm^{-1} indicate tetrahedral and octahedral occupancies of metal (M)–O bonds formed with the deposition of Co$_3$O$_4$ on GF electrodes, which suggests the formation of Co–O moieties in Co$_3$O$_4$–GF and PANI–Co$_3$O$_4$–GF.[48] The absorption band of C–H bending peaks for PANI shifts to higher peak positions in PANI–Co$_3$O$_4$–GF, which suggests a strong interaction between interweaved PANI and Co$_3$O$_4$ nanostructures on GF.[42] Furthermore, the broadening of the peak at 1306 cm^{-1} confirms the formation of a coordination compound between cobalt ions and amine/imine-nitrogen groups of PANI and enhanced charge delocalization on PANI with the incorporation of transition metal ions.[49]

Fig. 2c shows the XRD patterns for the four electrodes investigated. As shown, distinct diffraction patterns are observed at around 25.05°, 42.82°, 43.24°, and 52.48° assigned respectively to (002), (100), (101), and (102) planes of graphite (#).[50] Other carbon planes are observed at 37.24°, 62.64°, and 80.20°, which correspond to the turbostratic structure of carbon

(JCPDS no. 10-074-2330). The broad reflection from the (002) plane indicated the deprived crystallinity of GF.[51] The XRD spectrum of PANI–GF shows good crystallinity. In addition to the peaks of GF, new diffractions are observed at around 16.90° (011), 19.33°/20.49° (020), 25.16 (200), 27.39° (121), and 30.01° (022), which are assigned to reflection from (011), (020), (200), (121), and (022) planes of PANI (*).[52,53] Among these, the observed peaks at 19.33° and 25.16° correspond to the periodicity parallel and perpendicular to the long polymeric chains of PANI, suggesting a partially crystalline nature of the polymer.[54] The XRD spectrum of Co$_3$O$_4$–GF indicates reflections at 31.41°, 36.6°, 44.3°, and 54.54° attributed respectively to (220), (311), (400), and (422) planes of cobalt(II,III) oxide; Co$_3$O$_4$ (^) (JCPDS no. 00-074-1657).[55] The weak reflection at 62.54° is attributed to the (220) plane of cobalt(II) oxide; CoO (◆) (JCPDS card no. 43-1004).[56] The presence of Co$_3$O$_4$ peaks in the XRD spectrum of PANI–Co$_3$O$_4$–GF suggests that electro polymerization of PANI does not alter the crystalline structure of Co$_3$O$_4$. GF modified with cobalt oxide could act as an efficient platform to improve the anode mass transfer efficiency by enhancing the extracellular electron transfer in SMFCs, considering the excellent capacitive properties of Co$_3$O$_4$–GF that would act as an internal capacitor by accumulating the charge produced by the biofilm during the cell operation.[57] Sharp peaks at around 20° and 22.46° correspond to (110) and (003) lattice planes of PANI, respectively, confirming the amorphous state of the polyaniline deposited.[58]

SEM images of the four electrodes show structure changes. Despite harsh etching with acid and H$_2$O$_2$, GF fibers exhibit a smooth surface, which could be attributed to the limited oxidation ability of peroxide (Fig. 3a). The average diameter of

the microfibers increases from 13.1 µm for GF to 35.4 µm for PANI–GF, thus confirming the polymer deposition onto the GF fibers (Fig. 3b). Co_3O_4–GF shows a characteristic 3D flower-like nanostructure anchored on the GF fibers, which consists of many nanowires mounted together with sharp edges (Fig. 3c). Although the incorporation of transition metal oxides can enhance the electrical conductivity of anode electrodes in microbial fuel cells, they are typically characterised by a smooth surface and by poor corrosion resistance, which prevent the development of a good microbial biofilm.[59,60] The interweaving

of PANI and Co_3O_4–GF reveals a significant change in the electrode morphology, with a large density of defect sites, high porosity, and a rough surface that markedly enhance the electrode surface area (Fig. 3d). Microbial adhesion and charge diffusion are expected to be enhanced in PANI–Co_3O_4–GF.[61]

The elemental mapping of PANI–Co_3O_4–GF is assessed by energy dispersive X-ray spectroscopy (EDS) (Fig. 3e). As shown, cobalt, oxygen and nitrogen are uniformly distributed on the carbon matrix, thus suggesting that Co_3O_4 nanoflowers on the GF surface are covered by PANI with no phase segregation.[62]
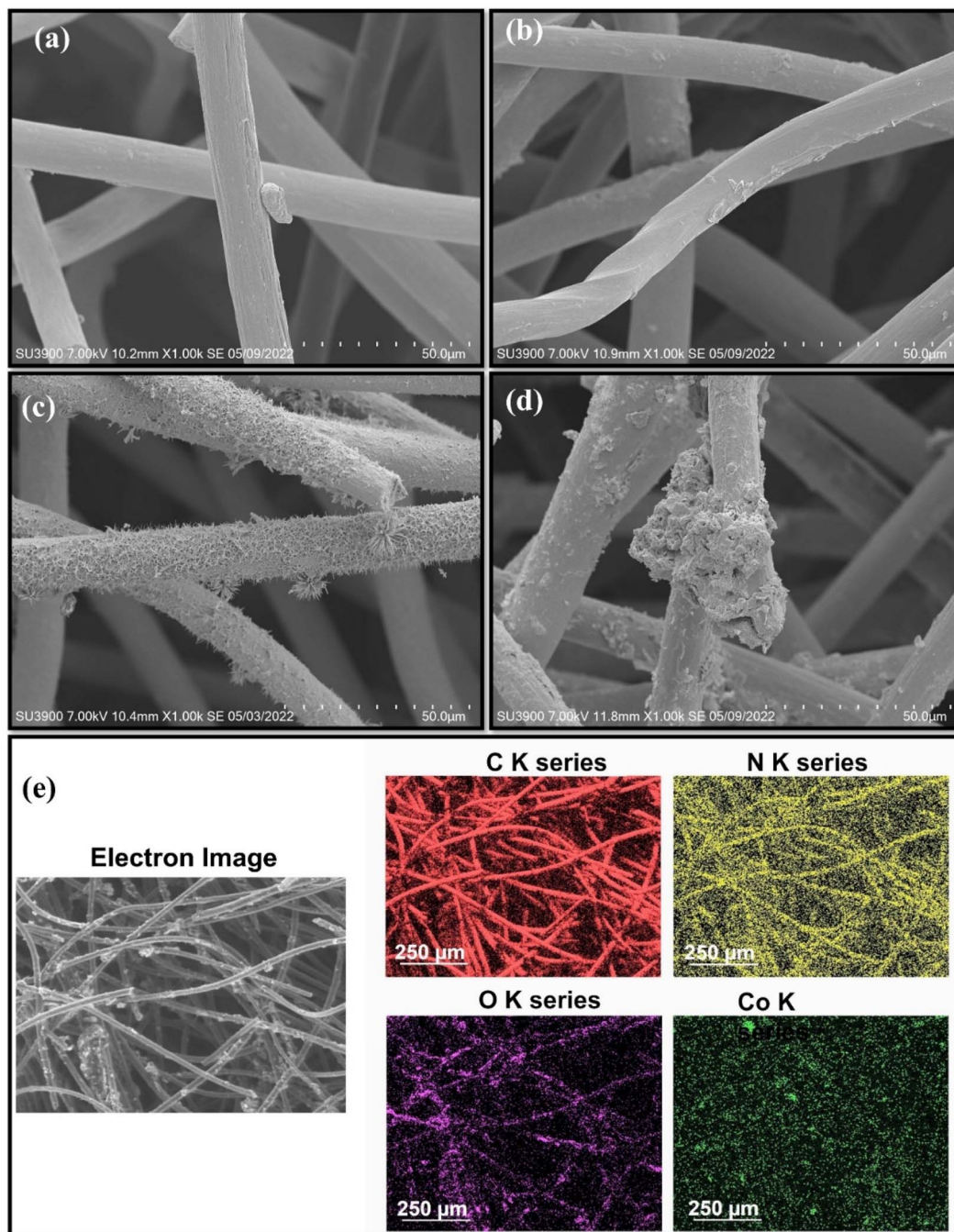
Fig. 3 SEM images of electrodes: (a) GF , (b) PANI–GF, (c) Co_3O_4–GF, and (d) PANI–Co_3O_4–GF. (e) Elemental mapping of PANI–Co_3O_4–GF.

Interweaving of PANI provides stability to Co_3O_4 by enhancing the interlayer distance to accommodate high ion density, thus increasing the specific capacity of the resulting composite electrode.[63] The elemental composition of PANI–Co_3O_4–GF is detailed in Table S1.†

3.2. Electrochemical performance of the anode electrodes developed

CV scans of the modified anodes prior to use in the SMFCs (Fig. 4a), revealed that PANI–GF generates the highest current density and largest area of the CV curve. This result suggests that the deposition of porous polyaniline enhances the double layer capacitance of the carbon electrode, with an increase in the charge storage.[64] PANI–Co_3O_4–GF shows a high redox potential, which could be a consequence of the synergistic effect of Co_3O_4 and PANI; this modification enhances the surface area of the electrode and its catalytic activity due to an increase in the density of active sites available for the redox reactions at the anode and an enhancement in the ion/electron diffusion rate.[65–67]

EIS spectra for the modified anodes were fitted to an equivalent circuit (Fig. 4b), consisting of ohmic resistance (R_1), charge transfer (or polarisation) resistance (R_2), constant phase element (Q), and Warburg resistance (W).[68] The ohmic resistance was recorded at around 11.05–13.55 Ω. The charge transfer resistance was the highest for PANI–GF, followed by PANI–Co_3O_4–GF, GF and Co_3O_4–GF. The high charge transfer resistance of PANI–GF could be a consequence of the steric hindrance towards ions induced with the deposition of polyaniline on graphite felt. PANI may hinder electron hopping, thus increasing the transition energy and decreasing the conductivity of the composite electrode, leading to high resistance.[69,70] Co_3O_4–GF showed the lowest resistance to charge transfer and good pseudo-capacitance for charge storage, which could be attributed to the extended surface area and high conductivity of Co_3O_4 that facilitate ion transport in the electrolyte.[71]

The catalytic activity of the biofilms on the anode electrodes was examined in SMFCs, implementing the four types of anodes in triplicate. In particular, the redox behaviour of the biofilm developed on the anode surface after 7, 30 and 60 days of operation was electrochemically characterized by CV. As shown in Fig. S1,† the CV curve recorded after 7 days of operation did not show any electrochemical activity. However, both the high current magnitudes and the increased CV curve area compared to those of GF suggest a superior electrochemical activity of modified anodes.[72] The electrocatalytic activity of the biofilms formed on several anode materials was tested after 30 and 60 days of SMFC operation. An increase in the CV curve area was observed for all electrodes, along with an increase in the capacitive current of the electrodes over time (Fig. 5). The CV surface area improvement indicates better extracellular electron transfer between the anode and the microbial biofilm.[61] PANI–GF exhibits an oxidation peak at −0.6 V, PANI–Co_3O_4–GF, at 0.56 V, Co_3O_4–GF, at 0.52 V, and GF, at 0.45 V, respectively. The peak current of PANI–Co_3O_4–GF was 12.12 mA, while Co_3O_4–GF recorded a current of 16.03 mA, followed by PANI–GF at 12.37 mA and GF at 8.83 mA. Compared to Co_3O_4–GF, the catalytic activity of PANI–Co_3O_4–GF was slightly lower. The highest peak and limiting current for Co_3O_4–GF suggest that Co_3O_4–GF could be a potential charge reservoir for efficient electron transfer due to its electrocapacitive behaviour.[73] Compared to Co_3O_4–GF, PANI–Co_3O_4–GF exhibits a lower capacitance and a greater electrochemical surface area (in terms of CV area).

CA analysis was conducted to measure the current produced as a function of anode modifications (Fig. 6a). The potential used in the CA tests was selected on the basis of the closed-circuit potential against the highest power output of PANI–Co_3O_4–GF from the polarization test conducted on day 7 of operation (measured to be 246.7 mV, Table S2†). As shown in Fig. 6a, a sharp drop in current was recorded, possibly due to the charging effect,[74] followed by a slow decrease rate. Co_3O_4–GF was characterized by the highest drop in the current of 5.6 mA, followed by PANI–GF (3.3 mA), PANI–Co_3O_4–GF (1.3 mA), and GF (0.5 mA). Although GF exhibits the lowest current drop,
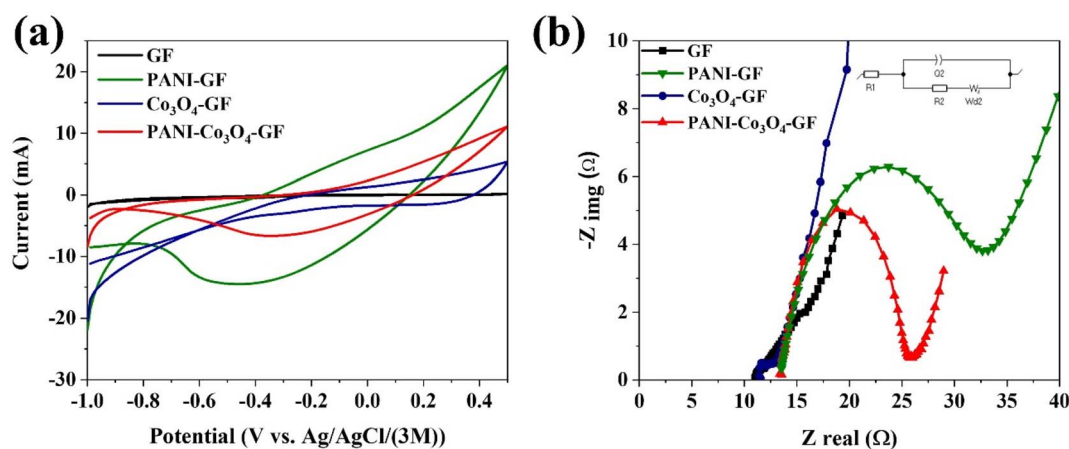

Fig. 4 Electrochemical characterisation of the anode electrodes before use. (a) CV scans at 0.01 V s^{-1} and (b) EIS spectra. Tests were performed in a 3-electrode system in 50 mM PBS (pH 7), with the anode as the working electrode and Pt wire (diameter: 0.127 mm) as the counter electrode.
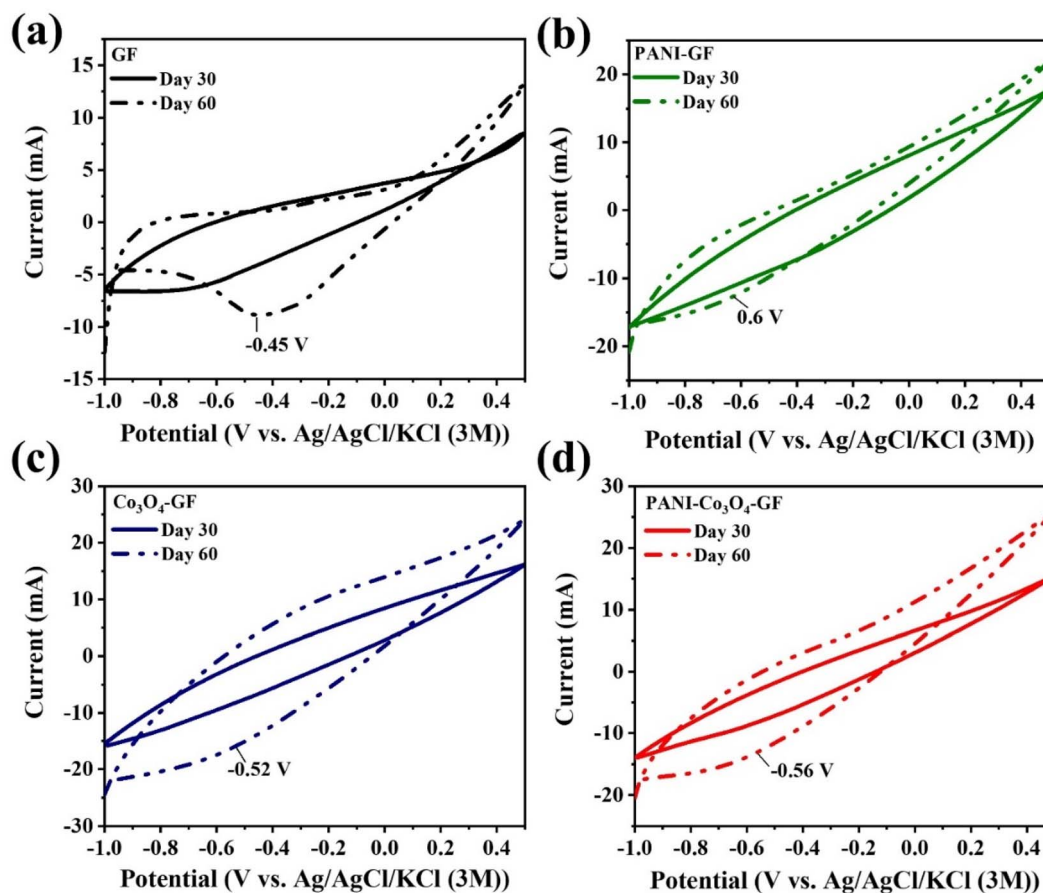
© 2023 The Author(s). Published by the Royal Society of Chemistry

Fig. 5 Comparison of CV scans at 0.01 V s^{-1} obtained with the anode tested in SMFCs operated for 30 and 60 days. (a) GF; (b) PANI–GF; (c) Co$_3$O$_4$–GF; (d) PANI–Co$_3$O$_4$–GF. Values are averages calculated from 3 replicate anodes with a maximum standard deviation of ±6.1 mA, ±2.4 mA, ±4.5 mA and ±4 mA, respectively.

the great value of the retention rate, which is a measure of the electrode durability, for PANI–Co$_3$O$_4$–GF (41.07%) compared to the other electrodes, suggests that GF functionalization with cobalt oxide and PANI leads to a material better suitable for long-term applications.[75] Among the several types of anodes tested, PANI–Co$_3$O$_4$–GF also records the highest current: 0.88 ± 14.5 mA (Table 2). LSV studies further confirm the better performance of PANI–Co$_3$O$_4$–GF (Fig. 6b and c). At a potential of 0.48 V, the absolute value of the limiting current increased by a factor of 1.6, compared to that for 30 days of operation, reaching a value of 27.07 ± 5.9 mA for PANI–Co$_3$O$_4$–GF after 60 days of operation while, Co$_3$O$_4$–GF, PANI–GF, and GF recorded a current of 31.91 ± 12.4 mA, 20.38 ± 9.3 mA, and 12.65 ± 2.8 mA on day 60 compared to 17.67 ± 18.6 mA, 16.61 ± 8.9 mA, and 14.17 ± 4.3 mA, on day 30, respectively.

As shown in Fig. 6d, after 4 months of operation in the SMFCs, both the ohmic and charge transfer resistance changed significantly for each electrode. The increase in the ohmic resistance is a consequence of testing the anodes in soil rather than in PBS. The solution resistance (R_1) for GF, PANI–GF, Co$_3$O$_4$–GF, and PANI–Co$_3$O$_4$–GF was recorded as 18.64 Ω, 18.18 Ω, 18.95 Ω, and 18.72 Ω, respectively. The charge transfer resistance (R_2) was the highest for GF, followed by PANI–GF, Co$_3$O$_4$–GF and PANI–Co$_3$O$_4$–GF (Table 3), implying that the

energy barrier for the redox reaction was the lowest for PANI–Co$_3$O$_4$–GF.[76] The substitution of O ions in Co$_3$O$_4$ and anions in PANI offers conducting holes, electron holes, and free electrons allowing the PANI chain to develop a potential gradient and consequently promote charge transfer to lower the internal resistance barrier for the redox reaction.[77] This improvement in the catalytic activity and electrode capacitance suggests that high active site density/defects on the electrode surface substantially improves the electron transfer in SMFCs.[78] The reaction kinetics of the pristine GF enriched with a biofilm is mainly controlled by charge transfer resistance; on the other hand, PANI–GF, Co$_3$O$_4$–GF, and PANI–Co$_3$O$_4$–GF show a combination of charge transfer resistance and pseudo capacitive properties.[79] The CV and EIS spectra for the anodes before and after operation, and therefore biofilm growth on the electrode surface, suggest that the redox active species within the biofilms have a positive effect on the extracellular electron transfer between the biofilms and the electrode surface.

3.3. Measurement of the performance of anode composites in SMFCs

Fig. S2 and S3† show the evolution of the anodic potential over time in SMFCs operated at closed-circuit potentials. After 60 s of
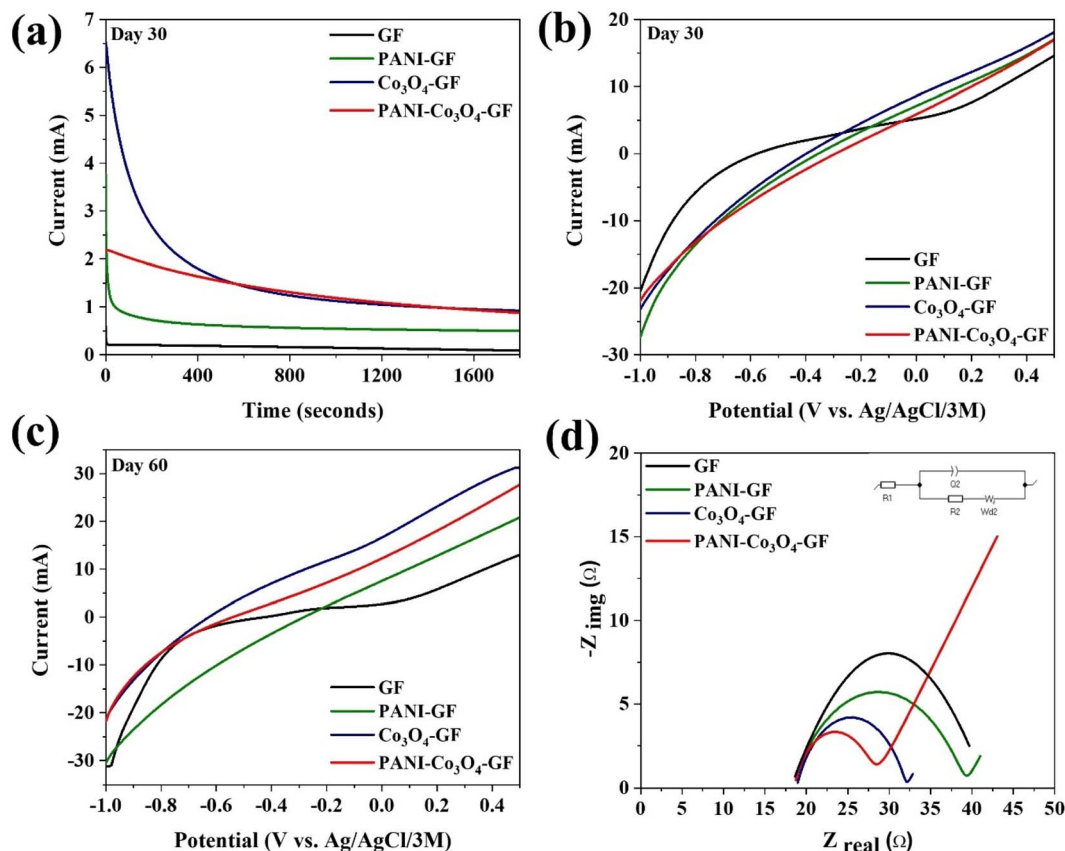
Fig. 6 Electrochemical characterisation of the four anodes during operation in SMFCs. (a) CA tests at 250 V after 30 days of operation. (b and c) LSV scans at a scan rate of 0.01 V s^{-1} after 30 and 60 days of operation. (d) EIS spectra of the anodes operated in SMFCs after four months of operation. Data in (a)–(c) are the averages of three replicates with a maximum standard deviation of ±3.1 mA, ±2.7 mA, ±1.5 mA and ±1.8 mA, respectively, for GF, PANI–GF, Co$_3$O$_4$–GF, and PANI–Co$_3$O$_4$–GF.

operation, the anode potential for PANI–Co$_3$O$_4$–GF drops from +312 mV to a stable potential of around −478 mV, while the Co$_3$O$_4$–GF anode recorded −406 mV, followed by PANI–GF at −363 mV and GF at −305 mV. Among the several anodes, PANI–

Co$_3$O$_4$–GF attains a negative potential in the shortest time (day 24), suggesting early biofilm formation and superior compatibility of the composite for biofilm enrichment.[78] Since, as expected, the performance of the cathode was similar in all

Table 2 Chronoamperometric values for the anodes (data refer to 3 replicates)

Anode material	Current at 0 s (i_0) mA	Current at 1800 s (i_{1800}) mA	(i_{1800})/(i_0)	Retention rate ($i_{1800} \times 100$)/i_0%
PANI–Co$_3$O$_4$–GF	2.13 ± 16.4	0.88 ± 14.5	0.4131 ± 0.9	41.31
PANI–GF	3.76 ± 23.8	0.50 ± 6.2	0.1329 ± 0.3	13.26
Co$_3$O$_4$–GF	6.52 ± 36.4	0.9 ± 19.4	0.1411 ± 0.5	14.11
GF	0.59 ± 9.6	0.09 ± 3.6	0.1525 ± 0.4	15.25

Table 3 Resistances from EIS tests of several anode electrodes before use and after 4 months of operation in SMFCs

Anode	In 50 mM PBS solution		In SMFCs (after 4 months)	
	Solution resistance (Ω)	Charge transfer resistance (Ω)	Solution resistance (Ω)	Charge transfer resistance (Ω)
GF	11.05	11.93	18.64	22.03
PANI–GF	13.38	18.92	18.18	21.04
Co$_3$O$_4$–GF	11.54	12.88	18.79	13.25
PANI–Co$_3$O$_4$–GF	13.54	12.01	18.52	9.58

devices tested (see polarisation curves of the cathode in Fig. S4(a)†), the performance difference in the several SMFCs can be attributed to the anode. PANI–Co$_3$O$_4$–GF showed the highest potential (in absolute value) amongst the several types of anodes tested, which favours the oxidation reactions at the anode with low charge transfer resistance, as shown in Fig. S4(b).† [79]

The power curves confirm the outperformance of the SMFCs with the PANI–Co$_3$O$_4$–GF anode. As shown in Fig. 7, except for the SMFC implementing the Co$_3$O$_4$–GF anode, the peak power density and the peak current density increased with time (Table S2†). In the case of the SMFC implementing the Co$_3$O$_4$–GF anode, after a 2.58 times increase in the power output after 30 days of operation, after 60 days of operation the increase with respect to day 7 was only 1.88 times. Contact angle measurements and CV studies confirm that Co$_3$O$_4$–GF exhibits low hydrophobicity and electrochemical surface area, leading to its better performance compared to plain GF. Nonetheless, the decrease in performance after 60 days of operation suggests poor stability of the electrode. PANI coating enhances the performance of plain GF, as the SMFC implementing the PANI–GF anode generated a peak power density 2.59 times higher than that of the SMFC with a plain GF anode after 60 days of operation. Moreover, PANI also contributes to stabilising Co$_3$O$_4$ on GF, as shown by the sustained greater performance of the SMFC implementing the PANI–Co$_3$O$_4$–GF anode.

The SMFC with the PANI–Co$_3$O$_4$–GF anode generated the maximum power density, with a peak value of 70.4 ± 1.4 mW
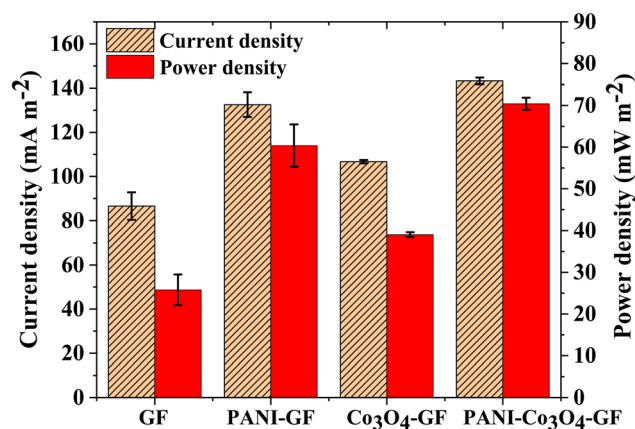
Fig. 8 Comparison of the power and current profile of the several SMFCs at 700 Ω on day 60 of operation. Error bars refer to three replicates.

m^{-2}, corresponding to a current density of 143.2 ± 1.4 mA m^{-2}. This corresponds to a 63.81% increase for the SMFC with the Co$_3$O$_4$–GF anode (42.9 ± 0.7 mW m^{-2}), a 16.62% increase over the SMFC with PANI–GF (60.4 ± 5.1 mW m^{-2}), and a 158.69% increase for the case of the SMFC with a GF anode (27.2 ± 3.7 mW m^{-2}) (Fig. 8). The high redox potential of PANI–Co$_3$O$_4$–GF favours the electron movement along the microbial transfer chains to the high potential anode, rendering them compatible for microbial adhesion.[80] The interweaving of polyaniline on Co$_3$O$_4$–GF resulted in better power performance, unlike
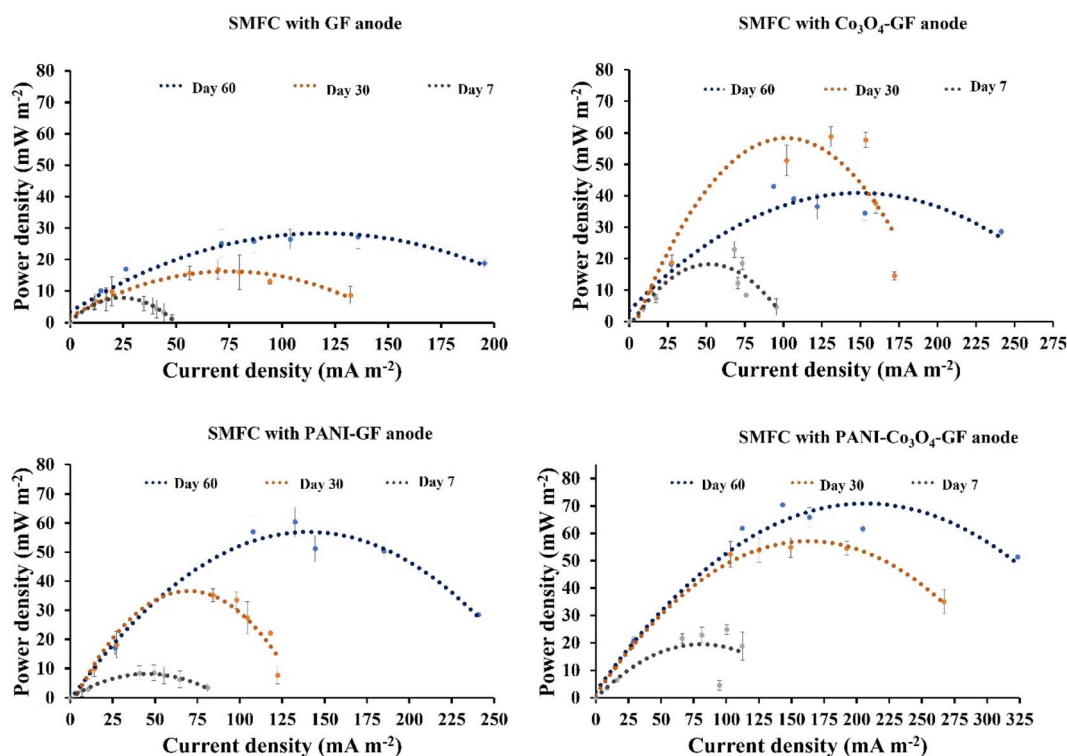
Fig. 7 Comparison of power curves obtained with the SMFCs implementing the different types of anode materials at 7, 30 and 60 days of operation. Error bars refer to three replicates.
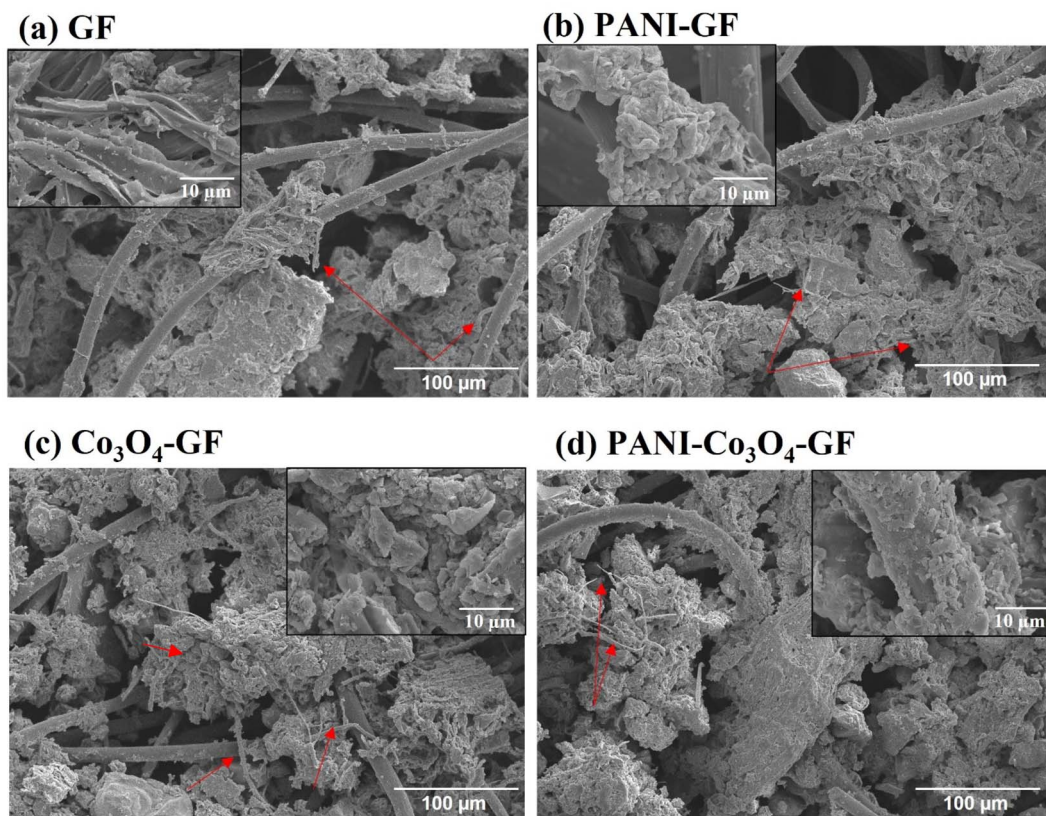
Fig. 9 SEM images of after 4 months of operation of the anodes: (a) GF, (b) PANI–GF, (c) Co_3O_4–GF, and (d) PANI–Co_3O_4–GF. Images were taken at 10 kV, with magnification 300. Red arrows in the images indicate filamentous assemblies.

a Co_3O_4–GF anode-based SMFC, where limited electron diffusion from the biofilm to the Co_3O_4–GF electrode suppressed the performance of the system with time.

The biofilm growth on anodes plays a crucial role in SMFCs for converting the chemical energy of the organics in soil to energy. The morphology of the biofilm developed on the anode surface was investigated by SEM. As shown in Fig. 9(a and b), the cell density was low on the surface of the GF and PANI–GF electrodes, while a more uniform biofilm coverage was observed in the case of Co_3O_4–GF (Fig. 9c) and PANI–Co_3O_4–GF (Fig. 9d). This result supports the hypothesis that Co_3O_4 nanoparticles improve the electrode biocompatibility and microbial adhesion.[79] The SEM images (Fig. 9c and d) reveal a highly dense biofilm, with a wide range of shape and size of microbes and filamentous microorganism assemblies colonizing the electrodes (marked with red arrows). The presence of such filaments is beneficial for connecting the felt fibres, thus enhancing the charge transfer between the biofilm and the electrode interface.[81] This dense and uniform coverage of PANI–Co_3O_4–GF with biofilm is due to an enhancement in the electrode's roughness and porosity and to a reduction in its hydrophobicity.[82] These results also suggest that the conductive-nanowire like filamentous microorganisms in the biofilm were well embedded in the composite matrix, boosting the extracellular electron transport in the SMFCs.

Further investigations, involving next generation sequencing, should be carry out in future work to assess if and how the functionalisation strategy proposed in this study influences the microbial composition of the anodic biofilm.

4. Conclusion

Soil microbial fuel cells have great potential as a renewable energy harvesting technology as well as a self-powered bioremediation strategy. Performance depends on the material and design of the electrodes implemented and, particularly in the case of the anode, a high specific surface area is key for the development of a high performing electroactive biofilm. In this study, graphite felt was functionalised with cobalt oxide and/or PANI to generate two different anode materials, Co_3O_4–GF and PANI–Co_3O_4–GF, tested for the first time in SMFCs. The performance of SMFCs implementing these anodes was compared, and benchmarked against two control SMFC devices, implementing a PANI functionalised GF anode (PANI–GF), to elucidate the effect of PANI on performance, and a plain GF anode. The highest power density was observed with the SMFC implementing the PANI–Co_3O_4–GF anode, with a peak power of 70 mW m^{-2} after 60 days of operation. This value was 1.6 times higher than the case of the Co_3O_4–GF anode, 1.3 times higher than the case of the SMFC with a PANI–GF anode, and 2.6 times higher than the case of the GF anode. Initially (up to

30 days of operation) the SMFC with the Co_3O_4–GF anode showed the best performance, however, the stability was poor; after 60 days of operation, the power density generated by the SMFC with the Co_3O_4–GF anode decreased by over 30% with respect to 30 days of operation, probably due to Co_3O_4 leaching. These results suggest that PANI has an important role in stabilising the Co_3O_4 nanostructure on the GF electrode surface. PANI also favours the development of a functional electrochemical biofilm, as demonstrated by the performance enhancement of the SMFC with the PANI–GF anode compared to the use of plain GF. While the cause for instability of the Co_3O_4–GF electrode must be better investigated, this study confirms the benefits of implementing metal oxide-conductive polymer composite electrode materials as anode in SMFCs for better performance, and accordingly inspires future trends in the field.

Author contributions

Simran Kaur Dhillon: conceptualization, investigation, methodology, electrochemical analysis, validation, data curation, writing – original draft, formal analysis. Jakub Dziegielowski: conceptualization and writing – data interpretation. Patit Paban Kundu: supervision, writing – review, editing. Mirella Di Lorenzo: supervision, conceptualization, data validation, and curation, writing – data interpretation and writing, funding securing.

Conflicts of interest

The authors declare no known competing financial interests.

Acknowledgements

References

1 R. Kumar, L. Singh, A. W. Zularisam and F. I. Hai, Microbial Fuel Cell Is Emerging as a Versatile Technology: A Review on Its Possible Applications, Challenges and Strategies to Improve the Performances, *Int. J. Energy Res.*, 2018, **42**(2), 369–394, DOI: **10.1002/er.3780**.

2 S. Bajracharya, M. Sharma, G. Mohanakrishna, X. Dominguez Benneton, D. P. B. T. B. Strik, P. M. Sarma and D. Pant, An Overview on Emerging Bioelectrochemical Systems (BESs): Technology for Sustainable Electricity, Waste Remediation, Resource Recovery, Chemical Production and Beyond, *Renewable Energy*, 2016, **98**, 153–170, DOI: **10.1016/j.renene.2016.03.002**.

3 J. Dziegielowski, B. Metcalfe, P. Villegas-Guzman, C. A. Martínez-Huitle, A. Gorayeb, J. Wenk and M. Di Lorenzo, Development of a Functional Stack of Soil Microbial Fuel Cells to Power a Water Treatment Reactor: From the Lab to Field Trials in North East Brazil, *Appl. Energy*, 2020, **278**, 115680, DOI: **10.1016/j.apenergy.2020.115680**.

4 E. Casula, B. Kim, H. Chesson, M. Di Lorenzo and M. Mascia, Modelling the Influence of Soil Properties on Performance and Bioremediation Ability of a Pile of Soil Microbial Fuel Cells, *Electrochim. Acta*, 2021, **368**, 137568, DOI: **10.1016/j.electacta.2020.137568**.

5 S. J. Dunaj, J. J. Vallino, M. E. Hines, M. Gay, C. Kobyljanec and J. N. Rooney-Varga, Relationships between Soil Organic Matter, Nutrients, Bacterial Community Structure, and the Performance of Microbial Fuel Cells, *Environ. Sci. Technol.*, 2012, **46**(3), 1914–1922, DOI: **10.1021/es2032532**.

6 I. Chicca, S. Becarelli and S. Di Gregorio, Microbial Involvement in the Bioremediation of Total Petroleum Hydrocarbon Polluted Soils: Challenges and Perspectives, *Environ. – MDPI*, 2022, **9**(4), 52, DOI: **10.3390/environments9040052**.

7 J. Dziegielowski, G. Bregu, L. Hulse and M. Di Lorenzo, Assessing the Effect of the Electrode Orientation on the Performance of Soil Microbial Fuel Cells, *E3S Web Conf.*, 2022, **334**, 08003, DOI: **10.1051/e3sconf/202233408003**.

8 Y. Sun, J. Wei, P. Liang and X. Huang, Electricity Generation and Microbial Community Changes in Microbial Fuel Cells Packed with Different Anodic Materials, *Bioresour. Technol.*, 2011, **102**(23), 10886–10891, DOI: **10.1016/j.biortech.2011.09.038**.

9 S. Z. Abbas and M. Rafatullah, Recent Advances in Soil Microbial Fuel Cells for Soil Contaminants Remediation, *Chemosphere*, 2021, **272**, 129691, DOI: **10.1016/j.chemosphere.2021.129691**.

10 S. K. Dhilllon, P. P. Kundu and R. Jain, Catalytic Advancements in Carbonaceous Materials for Bio-Energy Generation in Microbial Fuel Cells: A Review, *Environ. Sci. Pollut. Res.*, 2022, 0123456789, DOI: **10.1007/s11356-021-17529-9**.

11 H. Liu, R. Ramnarayanan and B. E. Logan, Production of Electricity during Wastewater Treatment Using a Single Chamber Microbial Fuel Cell, *Environ. Sci. Technol.*, 2004, **38**(7), 2281–2285, DOI: **10.1021/es034923g**.

12 R. Nitisoravut, C. N. D. Thanh and R. Regmi, Microbial Fuel Cells: Advances in Electrode Modifications for Improvement of System Performance, *Int. J. Green Energy*, 2017, **14**(8), 712–723, DOI: **10.1080/15435075.2017.1326049**.

13 B. Erable, N. Byrne, L. Etcheverry, W. Achouak and A. Bergel, Single Medium Microbial Fuel Cell: Stainless Steel and Graphite Electrode Materials Select Bacterial Communities Resulting in Opposite Electrocatalytic Activities, *Int. J. Hydrogen Energy*, 2017, **42**(41), 26059–26067, DOI: **10.1016/j.ijhydene.2017.08.178**.

14 C. Santoro, C. Arbizzani, B. Erable and I. Ieropoulos, Microbial Fuel Cells: From Fundamentals to Applications. A Review, *J. Power Sources*, 2017, **356**, 225–244, DOI: **10.1016/j.jpowsour.2017.03.109**.

15 S. Chen, J. Tang, L. Fu, Y. Yuan and S. Zhou, Biochar Improves Sediment Microbial Fuel Cell Performance in

Low Conductivity Freshwater Sediment, *J. Soils Sediments*, 2016, **16**(9), 2326–2334, DOI: **10.1007/s11368-016-1452-z**.

16 X. Li, X. Wang, Q. Zhao, L. Wan, Y. Li and Q. Zhou, Carbon Fiber Enhanced Bioelectricity Generation in Soil Microbial Fuel Cells, *Biosens. Bioelectron.*, 2016, **85**, 135–141, DOI: **10.1016/j.bios.2016.05.001**.

17 D. Pinto, T. Coradin and C. Laberty-Robert, Effect of Anode Polarization on Biofilm Formation and Electron Transfer in *Shewanella Oneidensis*/Graphite Felt Microbial Fuel Cells, *Bioelectrochemistry*, 2018, **120**, 1–9, DOI: **10.1016/j.bioelechem.2017.10.008**.

18 B. Yu, L. Feng, Y. He, L. Yang and Y. Xun, Effects of Anode Materials on the Performance and Anode Microbial Community of Soil Microbial Fuel Cell, *J. Hazard. Mater.*, 2021, **401**, 123394, DOI: **10.1016/j.jhazmat.2020.123394**.

19 W. Yang, X. Wang, M. Son and B. E. Logan, Simultaneously Enhancing Power Density and Coulombic Efficiency with a Hydrophobic Fe–N$_4$/Activated Carbon Air Cathode for Microbial Fuel Cells, *J. Power Sources*, 2020, **465**, 228264, DOI: **10.1016/j.jpowsour.2020.228264**.

20 A. Afkhami, T. Madrakian and Z. Karimi, The Effect of Acid Treatment of Carbon Cloth on the Adsorption of Nitrite and Nitrate Ions, *J. Hazard. Mater.*, 2007, **144**(1–2), 427–431, DOI: **10.1016/j.jhazmat.2006.10.062**.

21 S. K. Dhillon, A. Chaturvedi, D. Gupta, T. C. Nagaiah and P. P. Kundu, Copper Nanoparticles Embedded in Polyaniline Derived Nitrogen-Doped Carbon as Electrocatalyst for Bio-Energy Generation in Microbial Fuel Cells, *Environ. Sci. Pollut. Res.*, 2022, **29**(53), 80787–80804, DOI: **10.1007/s11356-022-21437-x**.

22 B. Yu, Y. Li and L. Feng, Enhancing the Performance of Soil Microbial Fuel Cells by Using a Bentonite-Fe and Fe$_3$O$_4$ Modified Anode, *J. Hazard. Mater.*, 2019, **377**, 70–77, DOI: **10.1016/j.jhazmat.2019.05.052**.

23 H. Xu, X. Quan, Z. Xiao and L. Chen, Effect of Anodes Decoration with Metal and Metal Oxides Nanoparticles on Pharmaceutically Active Compounds Removal and Power Generation in Microbial Fuel Cells, *Chem. Eng. J.*, 2018, **335**, 539–547, DOI: **10.1016/j.cej.2017.10.159**.

24 Q. Huang, P. Zhou, H. Yang, L. Zhu and H. Wu, *In Situ* Generation of Inverse Spinel CoFe$_2$O$_4$ Nanoparticles onto Nitrogen-Doped Activated Carbon for an Effective Cathode Electrocatalyst of Microbial Fuel Cells, *Chem. Eng. J.*, 2017, **325**, 466–473, DOI: **10.1016/j.cej.2017.05.079**.

25 X. Wang, W. Liu, H. Fu, X. H. Yi, P. Wang, C. Zhao, C. C. Wang and W. Zheng, Simultaneous Cr(vi) Reduction and Cr(iii) Removal of Bifunctional MOF/Titanate Nanotube Composites, *Environ. Pollut.*, 2019, **249**, 502–511, DOI: **10.1016/j.envpol.2019.03.096**.

26 V. Veeramani, K. Rajangam and J. Nagendran, Performance of Cobalt Oxide/Carbon Cloth Composite Electrode in Energy Generation from Dairy Wastewater Using Microbial Fuel Cells, *Sustainable Environ. Res.*, 2020, **30**(1), 7, DOI: **10.1186/s42834-020-00058-4**.

27 E. T. Kasem, T. Tsujiguchi and N. Nakagawa, Effect of Metal Modification to Carbon Paper Anodes on the Performance of Yeast-Based Microbial Fuel Cells Part II: In the Case with

Exogenous Mediator, Methylene Blue, *Key Eng. Mater.*, 2013, **534**, 82–87, DOI: **10.4028/www.scientific.net/KEM.534.82**.

28 B. Li and B. E. Logan, Bacterial Adhesion to Glass and Metal–Oxide Surfaces, *Colloids Surf., B*, 2004, **36**(2), 81–90, DOI: **10.1016/j.colsurfb.2004.05.006**.

29 M. Vagin, V. Gueskine, E. Mitraka, S. Wang, A. Singh, I. Zozoulenko, M. Berggren, S. Fabiano and X. Crispin, Negatively-Doped Conducting Polymers for Oxygen Reduction Reaction, *Adv. Energy Mater.*, 2021, **11**(3), 1–8, DOI: **10.1002/aenm.202002664**.

30 K. Dutta and P. P. Kundu, A Review on Aromatic Conducting Polymers-Based Catalyst Supporting Matrices for Application in Microbial Fuel Cells, *Polym. Rev.*, 2014, **54**(3), 401–435, DOI: **10.1080/15583724.2014.881372**.

31 C. Li, L. Zhang, L. Ding, H. Ren and H. Cui, Effect of Conductive Polymers Coated Anode on the Performance of Microbial Fuel Cells (MFCs) and Its Biodiversity Analysis, *Biosens. Bioelectron.*, 2011, **26**(10), 4169–4176, DOI: **10.1016/j.bios.2011.04.018**.

32 S. Kaur Dhillon and P. P. Kundu, Polyaniline Interweaved Iron Embedded in Urea-Formaldehyde Resin-Based Carbon as a Cost-Effective Catalyst for Power Generation in Microbial Fuel Cell, *Chem. Eng. J.*, 2021, 133341, DOI: **10.1016/j.cej.2021.133341**.

33 S. K. Dhillon and P. P. Kundu, Development of Polypyrrole Nanotube Coated with Chitosan and Nickel Oxide as a Biocompatible Anode to Enhance the Power Generation in Microbial Fuel Cell, *J. Power Sources*, 2022, **539**, 231595, DOI: **10.1016/j.jpowsour.2022.231595**.

34 H. O. Mohamed, M. A. Abdelkareem, M. Obaid, S. H. Chae, M. Park, H. Y. Kim and N. A. M. Barakat, Cobalt Oxides-Sheathed Cobalt Nano Flakes to Improve Surface Properties of Carbonaceous Electrodes Utilized in Microbial Fuel Cells, *Chem. Eng. J.*, 2017, **326**, 497–506, DOI: **10.1016/j.cej.2017.05.166**.

35 R. B. Song, K. Yan, Z. Q. Lin, J. S. Chye Loo, L. J. Pan, Q. Zhang, J. R. Zhang and J. J. Zhu, Inkjet-Printed Porous Polyaniline Gel as an Efficient Anode for Microbial Fuel Cells, *J. Mater. Chem. A*, 2016, **4**(38), 14555–14559, DOI: **10.1039/c6ta05770e**.

36 P. Zamani, D. Higgins, F. Hassan, G. Jiang, J. Wu, S. Abureden and Z. Chen, Electrospun Iron-Polyaniline-Polyacrylonitrile Derived Nanofibers as Non-Precious Oxygen Reduction Reaction Catalysts for PEM Fuel Cells, *Electrochim. Acta*, 2014, **139**, 111–116, DOI: **10.1016/j.electacta.2014.07.007**.

37 P. Champigneux, C. Renault-Sentenac, D. Bourrier, C. Rossi, M. L. Delia and A. Bergel, Effect of Surface Roughness, Porosity and Roughened Micro-Pillar Structures on the Early Formation of Microbial Anodes, *Bioelectrochemistry*, 2019, **128**, 17–29, DOI: **10.1016/j.bioelechem.2019.03.002**.

38 L. Zou, Y. Qiao, C. Zhong and C. M. Li, Enabling Fast Electron Transfer through Both Bacterial Outer-Membrane Redox Centers and Endogenous Electron Mediators by Polyaniline Hybridized Large-Mesoporous Carbon Anode

for High-Performance Microbial Fuel Cells, *Electrochim. Acta*, 2017, **229**, 31–38, DOI: 10.1016/j.electacta.2017.01.081.

39 Y. C. Yong, X. C. Dong, M. B. Chan-Park, H. Song and P. Chen, Macroporous and Monolithic Anode Based on Polyaniline Hybridized Three-Dimensional Graphene for High-Performance Microbial Fuel Cells, *ACS Nano*, 2012, **6**(3), 2394–2400, DOI: 10.1021/nn204656d.

40 C. Zhao, P. Gai, C. Liu, X. Wang, H. Xu, J. Zhang and J. J. Zhu, Polyaniline Networks Grown on Graphene Nanoribbons-Coated Carbon Paper with a Synergistic Effect for High-Performance Microbial Fuel Cells, *J. Mater. Chem. A*, 2013, **1**(40), 12587–12594, DOI: 10.1039/c3ta12947k.

41 X. Lin, Y. Shang, L. Li and A. Yu, Sea-Urchin-like Cobalt Oxide Grown on Nickel Foam as a Carbon-Free Electrode for Lithium–Oxygen Batteries, *ACS Sustainable Chem. Eng.*, 2015, **3**(5), 903–908, DOI: 10.1021/acssuschemeng.5b00012.

42 S. Narayanasamy and J. Jayaprakash, Carbon Cloth/Nickel Cobaltite ($NiCo_2O_4$)/Polyaniline (PANI) Composite Electrodes: Preparation, Characterization, and Application in Microbial Fuel Cells, *Fuel*, 2021, **301**, 121016, DOI: 10.1016/j.fuel.2021.121016.

43 F. Su, F. Wang, C. Zhang, T. Lu, S. Zhang, R. Zhang, X. Qi and P. Liu, Ameliorating Substance Accessibility for Microorganisms to Amplify Toluene Degradation and Power Generation of Microbial Fuel Cell by Using Activated Carbon Anode, *J. Cleaner Prod.*, 2022, **377**, 134481, DOI: 10.1016/j.jclepro.2022.134481.

44 K. Dujearic-Stephane, M. Gupta, A. Kumar, V. Sharma, S. Pandit, P. Bocchetta and Y. Kumar, The Effect of Modifications of Activated Carbon Materials on the Capacitive Performance: Surface, Microstructure, and Wettability, *J. Compos. Sci.*, 2021, **5**(3), 66, DOI: 10.3390/jcs5030066.

45 S. Gao, H. Mi, Z. Li, C. Ji, L. Sun, C. Yu and J. Qiu, Porous Polyaniline Arrays Oriented on Functionalized Carbon Cloth as Binder-Free Electrode for Flexible Supercapacitors, *J. Electroanal. Chem.*, 2019, **848**, 113348, DOI: 10.1016/j.jelechem.2019.113348.

46 J. Zhou, H. Zhang, T. Zuo, Q. Jia, L. Wang, Y. Tian, L. Gong, Y. Zhou and J. Wang, Enhanced Copper-Containing Wastewater Treatment with MnO_2/CNTs Modified Anode Microbial Fuel Cell, *Process Saf. Environ. Prot.*, 2022, **159**, 157–167, DOI: 10.1016/j.psep.2021.12.060.

47 J. Lu, B. A. Ayele, X. Liu and Q. Chen, Electrochemical Removal of RRX-3B in Residual Dyeing Liquid with Typical Engineered Carbonaceous Cathodes, *J. Environ. Manage.*, 2021, **280**, 111669, DOI: 10.1016/j.jenvman.2020.111669.

48 A. Medium, M. Ni, C. O. C. Synergism, T. Matthews, T. H. Dolla, S. S. Gwebu, T. A. Mashola, L. T. Dlamini, E. Carleschi, P. Ndungu and N. W. Maxakato, Mn-Ni-Co-O Spinel Oxides towards Oxygen Reduction Reaction in Alkaline Medium: $Mn_{0.5}Ni_{0.5}Co_2O_4$/C Synergism and Cooperation, *Catalysts*, 2021, **11**(9), 1059, DOI: 10.3390/catal11091059.

49 H. Xu, J. X. Wu, Y. Chen, J. L. Zhang and B. Q. Zhang, Facile Synthesis of Polyaniline/$NiCo_2O_4$ Nanocomposites with Enhanced Electrochemical Properties for Supercapacitors, *Ionics*, 2015, **21**(9), 2615–2622, DOI: 10.1007/s11581-015-1441-z.

50 B. Ilkiv, S. Petrovska, R. Sergiienko, O. Foya, O. Ilkiv, E. Shibata, T. Nakamura and Y. Zaulychnyy, Electronic Structure of Hollow Graphitic Carbon Nanoparticles Fabricated from Acetylene Carbon Black, *Fullerenes, Nanotubes, Carbon Nanostruct.*, 2015, **23**(5), 449–454, DOI: 10.1080/1536383X.2014.885957.

51 Z. Zhang, J. Xi, H. Zhou and X. Qiu, KOH Etched Graphite Felt with Improved Wettability and Activity for Vanadium Flow Batteries, *Electrochim. Acta*, 2016, **218**, 15–23, DOI: 10.1016/j.electacta.2016.09.099.

52 X. He, B. Gao, G. Wang, J. Wei and C. Zhao, A New Nanocomposite: Carbon Cloth Based Polyaniline for Anelectrochemical Supercapacitor, *Electrochim. Acta*, 2013, **111**, 210–215, DOI: 10.1016/j.electacta.2013.07.226.

53 D. J. Ahirrao, A. K. Pal, V. Singh and N. Jha, Nanostructured Porous Polyaniline (PANI) Coated Carbon Cloth (CC) as Electrodes for Flexible Supercapacitor Device, *J. Mater. Sci. Nanotechnol.*, 2021, **88**, 168–182, DOI: 10.1016/j.jmst.2021.01.075.

54 U. M. Casado, M. I. Aranguren and N. E. Marcovich, Preparation and Characterization of Conductive Nanostructured Particles Based on Polyaniline and Cellulose Nanofibers, *Ultrason. Sonochem.*, 2014, **21**(5), 1641–1648, DOI: 10.1016/j.ultsonch.2014.03.012.

55 J.-C. Mu, E.-Q. Wang, Y.-L. Zhang and L.-P. Zhang, A Novel and Green Synthesis of Mixed Phase $CoO@Co_3O_4@C$ Anode Material for Lithium Ion Batteries, *J. Nanosci. Nanotechnol.*, 2019, **19**(12), 7819–7825, DOI: 10.1166/jnn.2019.16744.

56 M. Montazerozohori, A. Masoudiasl, S. Farokhiyani, S. Joohari and P. McArdle, Sonochemical Synthesis of a New Cobalt(II) Complex: Crystal Structure, Thermal Behavior, Hirshfeld Surface Analysis and Its Usage as Precursor for Preparation of CoO/Co_3O_4 Nanoparticles, *Ultrason. Sonochem.*, 2017, **38**, 134–144, DOI: 10.1016/j.ultsonch.2017.03.017.

57 M. Rethinasabapathy, A. T. E. Vilian, S. K. Hwang, S. M. Kang, Y. Cho, Y. K. Han, J. K. Rhee and Y. S. Huh, Cobalt Ferrite Microspheres as a Biocompatible Anode for Higher Power Generation in Microbial Fuel Cells, *J. Power Sources*, 2021, **483**, 229170, DOI: 10.1016/j.jpowsour.2020.229170.

58 G. Mashao, K. D. Modibane, S. B. Mdluli, E. I. Iwuoha*, M. J. Hato, K. Makgopa and K. M. Molapo, Polyaniline-Cobalt Benzimidazolate Zeolitic Metal-Organic Framework Composite Material for Electrochemical Hydrogen Gas Sensing, *Electrocatalysis*, 2019, **10**(4), 406–419, DOI: 10.1007/s12678-019-00529-2.

59 T. Yamashita and H. Yokoyama, Molybdenum Anode: A Novel Electrode for Enhanced Power Generation in Microbial Fuel Cells, Identified *via* Extensive Screening of Metal Electrodes, *Biotechnol. Biofuels*, 2018, **11**(1), 1–13, DOI: 10.1186/s13068-018-1046-7.

60 T. Yin, Z. Lin, L. Su, C. Yuan and D. Fu, Preparation of Vertically Oriented TiO_2 Nanosheets Modified Carbon Paper Electrode and Its Enhancement to the Performance

of MFCs, *ACS Appl. Mater. Interfaces*, 2015, **7**(1), 400–408, DOI: **10.1021/am506360x**.

61 M. Farahmand Habibi, M. Arvand and S. Sohrabnezhad, Boosting Bioelectricity Generation in Microbial Fuel Cells Using Metal@metal Oxides/Nitrogen-Doped Carbon Quantum Dots, *Energy*, 2021, **223**, 120103, DOI: **10.1016/j.energy.2021.120103**.

62 H. R. Jiang, Y. K. Zeng, M. C. Wu, W. Shyy and T. S. Zhao, A Uniformly Distributed Bismuth Nanoparticle-Modified Carbon Cloth Electrode for Vanadium Redox Flow Batteries, *Appl. Energy*, 2019, **240**, 226–235, DOI: **10.1016/j.apenergy.2019.02.051**.

63 A. Ali, K. Hantanasirisakul, A. Abdala, P. Urbankowski, M. Q. Zhao, B. Anasori, Y. Gogotsi, B. Aïssa and K. A. Mahmoud, Effect of Synthesis on Performance of MXene/Iron Oxide Anode Material for Lithium-Ion Batteries, *Langmuir*, 2018, **34**(38), 11325–11334, DOI: **10.1021/acs.langmuir.8b01953**.

64 T. H. Han, N. Parveen, J. H. Shim, A. T. N. Nguyen, N. Mahato and M. H. Cho, Ternary Composite of Polyaniline Graphene and TiO_2 as a Bifunctional Catalyst to Enhance the Performance of Both the Bioanode and Cathode of a Microbial Fuel Cell, *Ind. Eng. Chem. Res.*, 2018, **57**(19), 6705–6713, DOI: **10.1021/acs.iecr.7b05314**.

65 C. Lei, F. Han, D. Li, W. C. Li, Q. Sun, X. Q. Zhang and A. H. Lu, Dopamine as the Coating Agent and Carbon Precursor for the Fabrication of N-Doped Carbon Coated Fe_3O_4 Composites as Superior Lithium Ion Anodes, *Nanoscale*, 2013, **5**(3), 1168–1175, DOI: **10.1039/c2nr33043a**.

66 X. Pan, W. Wang, Y. Chen, Q. Wen, X. Li, C. Lin, J. Wang, H. Xu and L. Yang, Bio-Electrocatalyst Fe_3O_4/Fe@C Derived from MOF as a High-Performance Bioanode in Single-Chamber Microbial Fuel Cell, *Biochem. Eng. J.*, 2022, **187**, 108611, DOI: **10.1016/j.bej.2022.108611**.

67 C. Zhang, P. Liang, X. Yang, Y. Jiang, Y. Bian, C. Chen, X. Zhang and X. Huang, Binder-Free Graphene and Manganese Oxide Coated Carbon Felt Anode for High-Performance Microbial Fuel Cell, *Biosens. Bioelectron.*, 2016, **81**, 32–38, DOI: **10.1016/j.bios.2016.02.051**.

68 S. B. Aziz, E. M. A. Dannoun, A. R. Murad, K. H. Mahmoud, M. A. Brza, M. M. Nofal, K. A. Elsayed, S. N. Abdullah, J. M. Hadi and M. F. Z. Kadir, Influence of Scan Rate on CV Pattern: Electrical and Electrochemical Properties of Plasticized Methylcellulose: Dextran (MC:Dex) Proton Conducting Polymer Electrolytes, *Alexandria Eng. J.*, 2022, **61**(8), 5919–5937, DOI: **10.1016/j.aej.2021.11.020**.

69 B. Martínez-Sánchez, D. Cazorla-Amorós and E. Morallón, Tailoring Intrinsic Properties of Polyaniline by Functionalization with Phosphonic Groups, *Polymers*, 2020, **12**(12), 1–18, DOI: **10.3390/polym12122820**.

70 P. Du, Y. Dong, H. Kang, X. Yang, Q. Wang, J. Niu, S. Wang and P. Liu, Graphene-Wrapped Polyaniline Nanowire Array Modified Functionalized of Carbon Cloth for High-Performance Flexible Solid-State Supercapacitor, *ACS Sustainable Chem. Eng.*, 2018, **6**(11), 14723–14733, DOI: **10.1021/acssuschemeng.8b03278**.

71 Y. Lu, X. Liu, W. Wang, J. Cheng, H. Yan, C. Tang, J. K. Kim and Y. Luo, Hierarchical, Porous CuS Microspheres Integrated with Carbon Nanotubes for High-Performance Supercapacitors, *Sci. Rep.*, 2015, **5**, 1–11, DOI: **10.1038/srep16584**.

72 A. Sumisha and K. Haribabu, Modification of Graphite Felt Using Nano Polypyrrole and Polythiophene for Microbial Fuel Cell Applications-a Comparative Study, *Int. J. Hydrogen Energy*, 2018, **43**(6), 3308–3316, DOI: **10.1016/j.ijhydene.2017.12.175**.

73 J. Li, C. Yao, B. Song, Z. Zhang and A. Libonati, Science of the Total Environment Enrichment of Sulfur-Oxidizing Bacteria Using S-Doped $NiFe_2O_4$ Nanosheets as the Anode in Microbial Fuel Cell Enhances Power Production and Sulfur Recovery, *Sci. Total Environ.*, 2022, **844**, 156973, DOI: **10.1016/j.scitotenv.2022.156973**.

74 S. K. Dhillon and P. P. Kundu, Magnesium Cobaltite Embedded in Corncob-Derived Nitrogen- Doped Carbon as a Cathode Catalyst for Power Generation in Microbial Fuel Cells, *ACS Appl. Mater. Interfaces*, 2022, **14**(42), 47633–47649, DOI: **10.1021/acsami.2c12279**.

75 K. Yoshii, K. Yamaji, T. Tsuda, H. Matsumoto, T. Sato, R. Izumi, T. Torimoto and S. Kuwabata, Highly Durable Pt Nanoparticle-Supported Carbon Catalysts for the Oxygen Reduction Reaction Tailored by Using an Ionic Liquid Thin Layer, *J. Mater. Chem. A*, 2016, **4**(31), 12152–12157, DOI: **10.1039/c6ta04859e**.

76 B. Tripathi, S. Pandit, A. Sharma, S. Chauhan, A. S. Mathuriya, P. K. Dikshit, P. K. Gupta, R. C. Singh, M. Sahni, K. Pant and S. Singh, Modification of Graphite Sheet Anode with Iron (II, III) Oxide-Carbon Dots for Enhancing the Performance of Microbial Fuel Cell, *Catalysts*, 2022, **12**(9), 1040, DOI: **10.3390/catal12091040**.

77 D. Z. Sun, Y. Y. Yu, R. R. Xie, C. L. Zhang, Y. Yang, D. D. Zhai, G. Yang, L. Liu and Y. C. Yong, *In Situ* Growth of Graphene/Polyaniline for Synergistic Improvement of Extracellular Electron Transfer in Bioelectrochemical Systems, *Biosens. Bioelectron.*, 2017, **87**, 195–202, DOI: **10.1016/j.bios.2016.08.037**.

78 P. Champigneux, C. Renault-Sentenac, D. Bourrier, C. Rossi, M.-L. Délia-Dupuy and A. Bergel, Effect of Surface Roughness, Porosity and Roughened Micro-Pillar Structures on the Early Formation of Microbial Anodes, *Bioelectrochemistry*, 2019, **128**, 17–29, DOI: **10.1016/j.bioelechem.2019.03.002ï**.

79 R. P. Ramasamy, Z. Ren, M. M. Mench and J. M. Regan, Impact of Initial Biofilm Growth on the Anode Impedance of Microbial Fuel Cells, *Biotechnol. Bioeng.*, 2008, **101**(1), 101–108, DOI: **10.1002/bit.21878**.

80 S. Khilari, S. Pandit, J. L. Varanasi, D. Das and D. Pradhan, Bifunctional Manganese Ferrite/Polyaniline Hybrid as Electrode Material for Enhanced Energy Recovery in Microbial Fuel Cell, *ACS Appl. Mater. Interfaces*, 2015, **7**(37), 20657–20666, DOI: **10.1021/acsami.5b05273**.

81 L. Jourdin, S. M. T. Raes, C. J. N. Buisman and D. P. B. T. B. Strik, Critical Biofilm Growth throughout Unmodified Carbon Felts Allows Continuous

Bioelectrochemical Chain Elongation from CO_2 up to Caproate at High Current Density, *Front. Energy Res.*, 2018, **6**, 1–15, DOI: **10.3389/fenrg.2018.00007**.

82 B. Thulasinathan, S. Nainamohamed, J. O. Ebenezer Samuel, S. Soorangkattan, J. B. Muthuramalingam, M. Kulanthaisamy, R. Balasubramani, D. D. Nguyen, S. W. Chang, N. Bolan, Y. F. Tsang, L. E. Amabilis-Sosa and A. Alagarsamy, Comparative Study on Cronobacter Sakazakii and Pseudomonas Otitidis Isolated from Septic Tank Wastewater in Microbial Fuel Cell for Bioelectricity Generation, *Fuel*, 2019, **248**, 47–55, DOI: **10.1016/j.fuel.2019.03.060**.